HHS Public Access

Author manuscript

Dev Biol. Author manuscript; available in PMC 2017 January 15.

Published in final edited form as:

Dev Biol. 2016 January 15; 409(2): 429–441. doi:10.1016/j.ydbio.2015.11.017.

A three-dimensional study of alveologenesis in mouse lung

Kelsey Branchfield[a], **Rongbo Li**[a], **Vlasta Lungova**[b], **Jamie M. Verheyden**[a], **David McCulley**[c], and **Xin Sun**[a,*]

[a]Laboratory of Genetics, University of Wisconsin-Madison Madison, WI 52706, United States

[b]Department of Surgery, University of Wisconsin-Madison Madison, WI 53706, United States

[c]Department of Pediatrics University of Wisconsin-Madison Madison, WI 53706, United States

Abstract

Alveologenesis is the final step of lung maturation, which subdivides the alveolar region of the lung into smaller units called alveoli. Each of the nascent dividers serves as a new gas-exchange surface, and collectively they drastically increase the surface area for breathing. Disruption of alveologenesis results in simplification of alveoli, as is seen in premature infants diagnosed with bronchopulmonary dysplasia (BPD), a prevalent lung disease that is often associated with lifelong breathing deficiencies. To date, a majority of studies of alveologenesis rely on two-dimensional (2D) analysis of tissue sections. Given that an overarching theme of alveologenesis is thinning and extension of the epithelium and mesenchyme to facilitate gas exchange, often only a small portion of a cell or a cellular structure is represented in a single 2D plane. Here, we use a three-dimensional (3D) approach to examine the structural architecture and cellular composition of myofibroblasts, alveolar type 2 cells, elastin and lipid droplets in normal as well as BPD-like mouse lung. We found that 2D finger-like septal crests, commonly used to depict growing alveolar septae, are often artifacts of sectioning through fully established alveolar walls. Instead, a more accurate representation of growing septae are 3D ridges that are lined by platelet-derived growth factor receptor alpha (PDGFRA) and alpha smooth muscle actin (α-SMA)-expressing myofibroblasts, as well as the elastin fibers that they produce. Accordingly in 3D, both α-SMA and elastin were each found in connected networks underlying the 3D septal ridges rather than as isolated dots at the tip of 2D septal crests. Analysis through representative stages of alveologenesis revealed unappreciated dynamic changes in these patterns. PDGFRA-expressing cells are only α-SMA-positive during the first phase of alveologenesis, but not in the second phase, suggesting that the two phases of septae formation may be driven by distinct mechanisms. Thin elastin fibers are already present in the alveolar region prior to alveologenesis, suggesting that during alveologenesis, there is not only new elastin deposition, but also extensive remodeling to transform thin and uniformly distributed fibers into thick cables that rim the nascent septae. Analysis of several genetic as well as hyperoxia-induced models of BPD revealed that the myofibroblast organization is perturbed in all, regardless of whether the origin of defect is epithelial, mesenchymal, endothelial or environmental. Finally, analysis of relative position of PDGFRA-positive cells and alveolar type 2 cells reveal that during alveologenesis, these two cell types are

*Corresponding author. xsun@wisc.edu (X. Sun).

Appendix A. Supplementary material

Supplementary data associated with this article can be found in the online version at http://dx.doi.org/10.1016/j.ydbio.2015.11.017.

not always adjacent to one another. This result suggests that the niche and progenitor relationship afforded by their close juxtaposition in the adult lung may be a later acquired property. These insights revealed by 3D reconstruction of the septae set the foundation for future investigations of the mechanisms driving normal alveologenesis, as well as causes of alveolar simplification in BPD.

Keywords

Lung; Development; Mouse; Alveologenesis

1. Introduction

A cardinal goal of lung development is to produce sufficient surface area for gas exchange. Prenatally, the lung undergoes over 20 generations of branching, which is followed by formation of saccules at the distal ends of branches. These saccules will then be subdivided into gas-exchange units called alveoli. Alveoli formation, or alveologenesis, occurs primarily postnatally with 90% of human alveoli and all of mouse alveoli forming after birth (Churg et al., 2005). In mice, alveologenesis initiates at ~postnatal day 4 (P4), peaks at ~P7 and ends at ~P36 (Mund et al., 2008; Schittny et al., 2008). In human, alveologenesis initiates at ~32 weeks of gestation, and continues until ages 2 through 8, depending on estimation (Dunnill, 1962; Langston et al., 1984; Thurlbeck, 1982). In human lungs, alveologenesis will generate over 300 million alveoli which constitute approximately 75 m^2 alveolar surface area (Ochs et al., 2004; Rhoades and Bell, 2012). Alveologenesis is critical for proper lung function, but the underlying mechanisms governing this process are poorly understood.

Among all steps of lung development, alveologenesis is the most frequently perturbed process in lung diseases. Disruptions in alveolar formation are often observed in very low birth weight premature infants resulting in a life-long disease called bronchopulmonary dysplasia (BPD) (Husain et al., 1998; Jobe, 1999). Due to a halt in lung maturation and inability to breathe on their own, these infants need to be ventilated with positive-pressure oxygen, which further damages alveolar structures (Askie et al., 2003; Jobe and Bancalari, 2001; Saugstad, 2003; Vento et al., 2009). BPD is often studied using a mouse models by treating neonatal wildtype pups with hyperoxia. However, much still need to be learned about the complex molecular and cellular causes of alveolar simplification in BPD.

Alveologenesis requires spatial and temporal coordination of multiple specialized cell types (Greer et al., 2014). In the alveolar epithelium, alveolar epithelial type1 cells (AEC1s) line the alveolus and form the air-blood barrier. Alveolar epithelial type 2 cells (AEC2s) secrete surfactants, which reduce surface tension and prevent collapse of the alveolar wall upon expiration. It is believed that the alveolar mesenchyme contains multiple types of fibroblast populations. While all are poorly characterized, two of which are loosely defined as myofibroblasts, which exhibit contractile properties and produce elastin, and lipofibroblasts, which contain lipid droplets (Adler et al., 1989; Brody and Kaplan, 1983; Kapanci et al., 1974; McGowan and Torday, 1997; Mitchell et al., 1990; Rehan et al., 2006). The

microvasculature of the lung includes both the capillary network, through which blood is oxygenated, and the lymphatic network through which excess fluid is drained. Most of the aforementioned alveolar cell types are required for septation. However, little is known about the specific role of each population and how they coordinate their function to achieve alveologenesis.

In this study, we focused on the alveolar myofibroblasts, as they are thought to play a key role in septation (Boström et al., 1996; Lindahl et al., 1997; McGowan et al., 2008). Myofibroblasts are defined by their expression of alpha-smooth muscle actin (α-SMA, also termed ACTA2), which is thought to drive myofibroblast contraction observed *in vitro* (Adler et al., 1989; Arora et al., 1999; Chen et al., 2012; Leslie et al., 1990; McGowan et al., 2008; Sanders et al., 2007). Myofibroblasts are believed to be the primary producer of elastin, an extracellular matrix molecule (Boström et al., 1996; Lindahl et al., 1997). Elastin fiber elasticity allows the lung to stretch during inhalation and recoil afterwards.

Many questions remain in regard to myofibroblast differentiation and function. It is generally believed that *Pdgfra* is a marker of myofibroblast precursors and myofibroblasts. At the end of sacculation and in preparation for alveologenesis (P0–P3), $PDGFRA^+$ myofibroblast precursors are believed to migrate from the saccule openings distally around the saccule to future sites of septae initiation. In *Pdgfa−/−* mutant, this migration does not occur and no septae forms (Boström et al., 1996; Lindahl et al., 1997; McGowan et al., 2008). While it is believed that PDGFA signaling is mediated via PDGFRA, a similar failure of myofibroblast precursor positioning phenotype has not been shown in any *Pdgfra* mutants that have been analyzed (Boström et al., 2002; McGowan and McCoy, 2014, 2013). During alveologenesis, it is proposed that $PDGFRA^+$ myofibroblasts migrate from the base of the saccule towards the lumen (Burri, 1984; Lindahl et al., 1997; Prodhan and Bernard Kinane, 2002). As a result, myofibroblasts are found at the alveolar entrance ring (AER) which rims the nascent septal cup (McGowan et al., 2008). However, it remains unclear what propels the myofibroblasts into the lumen.

Current models of alveologenesis have focused on two-dimensional (2D) sections of the alveoli. These studies have identified structures called secondary septal crests, which are finger-like protrusions into the lumen thought to be the growing structures that subdivide saccules into alveoli (Amy et al., 1977; Burri, 1984; Zeltner and Burri, 1987). Since these crests often contain elastin, it is hypothesized that elastin deposition into crest tips drives septation (Boström et al., 1996; Burri and Weibel, 1977; Burri, 1984; Emery, 1970; Noguchi et al., 1989). However, when the luminal surface of the alveolar region was viewed by 3D synchrotron-radiation x-ray tomography, no finger-like protrusions were observed (Mund et al., 2008; Schittny et al., 2008). Instead, long ridges appear to rise up from the saccule walls into the airspace. These results led us to question how the 2D septal crest corresponds to the structures observed during alveolar formation in 3D. Therefore, we sought to characterize the architecture and cellular composition of the lung just before and during alveologenesis using 3D reconstruction.

2. Results

2.1. Alveolar “septal crests” are an artifact of 2D sectioning and 3D septal ridges are lined with a network of α-SMA fibers

To visualize alveoli in 3D throughout lung maturation, we imaged ~70 μm lung slices immunostained for various alveolar cell and matrix markers between P0 and P15, which precedes and contains the peak window of alveologenesis (Mund et al., 2008; Schittny et al., 2008). Staining for AEC1s with T1α antibody provided a clear outline of the alveolar architecture (Fig. 1). As expected, many septal crests were visible in 2D at P7, a peak stage of alveologenesis (Fig. 1A–C). Nearly all septal crest tips exhibited α-SMA expression (Fig. 1A–C). In serial optical sections, we noticed that septal crests joined to form continuous alveolar walls in adjacent optical planes (Fig. 1A–C, arrows). In fact, most septal crests viewed in one optical plane converged into continuous alveolar walls only 2–5 μm lower. When the 2D series was rendered in 3D, alveoli appeared as cup-like structures lined by AEC1s with an open side facing the air-filled lumen. There were no visible fingerlike septal crests (Fig. 1D and E, Movie S1). Rather, many previously identified septal crests were in fact part of an existing fully grown septal ridge, where the optical section had transected the ridge and exposed the cut surface (Fig. 1D and E, arrows, also as diagrammed in Fig. 7A–C). Thus, rather than septa crests in 2D, septal ridges in 3D are more accurate representations of growing surfaces that subdivide the alveoli. Interestingly, we found that septal ridges, some in the form of circular rims at the alveolar entrance ring (AER), were all lined by α-SMA fibers at P7.

Supplementary material related to this article can be found online at http://dx.doi.org/10.1016/j.ydbio.2015.11.017.

2.2. α-SMA is expressed in a restricted window during alveologenesis

Since myofibroblasts are thought to drive alveologenesis, we next used α-SMA as a marker and imaged these cells prior to and during alveologenesis in 3D. In addition, we used *Pdgfra* as it has been implicated as a marker for both the myofibroblast precursor as well as for myofibroblasts (Boström et al., 1996; McGowan et al., 2008; Perl and Gale, 2009). We carried out the α-SMA antibody staining in lungs from $Pdgfra^{H2B\text{-}GFP/+}$ mice (hereafter PDGFRA-GFP), where H2B-eGFP is expressed from the endogenous *Pdgfra* locus, labeling the nuclei (Hamilton et al., 2003; Kimani et al., 2009). At P0, prior to the initiation of alveologenesis, α-SMA fibers were observed in a subset of the PDGFRA-GFP$^+$ cells that surrounded the saccule openings, but they were only observed in low intensity in the PDGFRA-GFP$^+$ cells dispersed throughout the interstitial mesenchyme (Fig. 2A, Fig. S1A). Starting at P2, α-SMA fibers were detected in the alveolar interstitium (Fig. S2A$_i$).

At P7, α-SMA$^+$ fibers were observed in all PDGFRA-GFP$^+$ cells, both surrounding large saccule openings as well as around the ridges of alveoli, regardless of whether the GFP is bright or dim (Fig. 2B, S1B, S2B$_i$). Approximately 3–7 PDGFRA-GFP$^+$ myofibroblasts surround each alveolus with α-SMA fibers that appear to encircle the AER (also as diagrammed in Fig. 7E). It is interesting that no gaps were clearly visible in these α-SMA$^+$ rings, even though α-SMA fibers are contained within myofibroblast cells, and presumably

are not continuous across cell-cell junctions (Fig. 2B, S2B$_{i}$, Movie S2). This suggests that myofibroblasts may form elongated cytoplasmic protrusions and tight or overlapping connections to establish a continuous loop around the AER. Furthermore, these rings appear interconnected with each other, giving rise to a “fishnet”-like α-SMA network.

Supplementary material related to this article can be found online at http://dx.doi.org/10.1016/j.ydbio.2015.11.017.

Immunostaining showed that myofibroblasts also express SM22 (also termed Transgelin), another smooth muscle marker (Fig. S2Bii, Biii). At P7, SM22 staining was present throughout the cytoplasm of myofibroblasts, overlapping with both α-SMA fibers and PDGFRA-GFP^{+} nuclei (Fig. S2B$_{ii}$, B$_{iii}$). SM22 staining, like α-SMA staining, showed that myofibroblasts are tightly connected forming rings around each alveolus at P7. Slightly lower intensity of α-SMA fibers continue to be detected in all PDGFRA-GFP^{+} cells through P12, consistent with published findings (McGowan et al., 2008) (Fig. S2A$_{vii}$).

By P15, no α-SMA fibers were present in the alveolar region while abundance of PDGFRA-GFP^{+} nuclei remain (Fig. 2C and S1C). α-SMA^{+} smooth muscle is only observed surrounding proximal airways, including terminal bronchioles (Fig. 2C). SM22 staining intensity is also reduced and becomes uneven, in contrast to that at P7 (Fig. S2D). In the adult lung sampled at P40, α-SMA staining intensity continues to be low in the alveolar region while PDGFRA-GFP^{+} nuclei remain abundant (Fig. S1D). The temporal changes in α-SMA staining intensity are corroborated by quantitative RT-PCR (qRT) and western-blot data measuring the levels of α-SMA transcript as well as protein, respectively (Fig. S3). These results suggest that the changes in staining intensity are due to changes in expression level. We also analyzed general filamentous actin (F-actin) pattern using phalloidin staining at the same stages (Fig. S1E–H). As expected, phalloidin staining is detected in all cells in the alveolar region. There appear to be a slight overall downregulation of intensity and fewer labeled long fibers at P15 and P40 compared to earlier stages. These results suggest that the myofibroblast characteristic as defined by α-SMA staining is a transient feature of PDGFRA-GFP^{+} alveolar fibroblasts.

2.3. Increased α-SMA fibers represent a general stress response to impaired lung maturation

To determine the role of myofibroblasts in the pathogenesis of impaired alveolar formation, we characterized myofibroblasts in several models using the 3D approach. We assessed genetic mutant models with primary defects in each of the major cell lineages of the lung—the epithelium, the endothelium and the myofibroblasts. In addition, we assessed myofibroblasts in wild-type mice treated with hyperoxia from birth, a commonly used model of BPD (Fig. 3).

For the endothelial mutant, we used a null allele of *Pecam-1*, which encodes a cell adherens junction protein expressed on the surface of endothelial cells. *Pecam1* mutant mice show impaired alveologenesis as a result of defects in endothelial cell migration, but not cell proliferation or survival (DeLisser et al., 2006) (Fig. 3A and B). For the epithelial mutant, we used the *Shhcre;Etv4;5* mutant, where two paralogous transcription factor genes

downstream of FGF pathway, are inactivated in the epithelium by *Shhcre* (Fig. 3C and D). These mutant mice show defects in epithelial branching followed by saculation and alveologenesis as a result of altered gene expression in the epithelium (Herriges et al., 2015). For the mesenchymal mutant, we used the *Tbx4cre;Pdgfra*$^{GFP/fl}$ mutant, where *Pdgfra*, the receptor which is not only a marker, but also is essential for myofibroblast function, is inactivated in the mesenchyme using one *Pdgfra* allele where GFP has been knocked into the endogenous locus disrupting gene function, and one floxed *Pdgfra* allele inactivated by *Tbx4cre* in the lung mesenchyme (Hamilton et al., 2003; Klinghoffer et al., 2002; McGowan and McCoy, 2013; Naiche et al., 2011) (Fig. 3E and F). It has been shown previously, and we confirmed that *Tbx4cre* has widespread activity in the lung mesenchyme (Fig. S4) (Naiche et al., 2011). This allelic combination allows us to both inactivate *Pdgfra* in the mesenchyme and simultaneously visualize the remaining myofibroblasts. *Tbx4cre;Pdgfra*$^{GFP/fl}$ mutants show a strong alveolar simplification phenotype similar to that observed when *Pdgfra* is inactivated in the smooth muscle cells by Transgelin-cre (McGowan and McCoy, 2013) (Fig. S5). For the hyperoxia exposure model, we placed 1-day old *Pdgfra*$^{GFP/+}$ pups into a 75% oxygen environmental chamber for 2 weeks and then analyzed lungs at P15 (Fig. 3G and H). Similar treatment has been shown to mimic features of human BPD (Aslam et al., 2009; Bozyk et al., 2012; Ratner et al., 2009).

We were surprised to find that all models exhibited increased and disorganized α-SMA fiber staining compared to normal controls (Fig. 3A–H). In the hyperoxia-exposed lungs, as we analyzed the lungs after the two-week regime, we examined them at a stage when α-SMA is no longer expressed in the alveolar region in mice raised in normoxic conditions (P15). In hyperoxia-exposed mice, however, α-SMA continued to be detected, although the number and distribution of PDGFRA-GFP expressing myofibroblasts appeared normal (Fig. 3G and H). This finding that the increase and disorganization of α-SMA fibers can be observed in the distinct mutants and following hyperoxia treatment suggest that the myofibroblast phenotype is a general response to disruptions of lung maturation, and may be the common effector leading to the shared outcome of alveoli simplification.

PDGFA signaling has been proposed to provide a migratory signal for myofibroblasts distribution around the saccule in preparation for septae formation (Boström et al., 1996; Lindahl et al., 1997; McGowan et al., 2008). This is based on the finding that in *Pdgfa* mutants, *Pdgfra*-expressing myofibroblast precursor cells are stalled at the openings of the saccules, and are not able to migrate into the saccules. As the principle PDGFA receptor is PDGFRA, we addressed whether conditional inactivation of *Pdgfra* in the lung mesenchyme would lead to a similar defect as the ligand mutant. In *Tbx4cre;Pdgfra* mutant lungs, PDGFRA-GFP^{+} myofibroblasts appeared widely distributed throughout the alveolar region (Fig. 3E and F, S6). We did not observe any preferential clustering of myofibroblasts either near saccule openings, or at the bases of alveoli, suggesting that there is no defect in myofibroblast distribution in this receptor mutant.

2.4. Elastin fiber network is established prior to alveologenesis and undergoes remodeling, not just de novo deposition, during alveologenesis

Since myofibroblast deposition of elastin is viewed as a critical component of septation, we characterized the dynamic changes of the elastin fiber matrix in 3D (Boström et al., 1996; Burri and Weibel, 1977; Burri, 1984; Emery, 1970; Noguchi et al., 1989). We were surprised to find that at birth, PDGFRA-GFP$^+$ cells have already established a complex elastin fiber network that not only surrounds saccules but also is distributed throughout the interstitium (Fig. 4A). All PDGFRA-GFP$^+$ cells appear to be closely associated with elastin fibers at P0, consistent with the possibility that they are the primary elastin producing cells. By P7, the elastin network appears significantly remodeled with fewer thin fibers and a tighter localization of elastin bundles specifically encircling alveolar openings (Fig. 4B, $S2B_{iv}$, Movie S3). At this stage, elastin and α-SMA fibers formed closely parallel networks (Fig. $S6_{Aiii}$, A_{vi}, A_{ix}, C, Movie S4), suggesting that myofibroblasts may drive elastin remodeling. By P15, unlike the disappearance of α-SMA, the elastin network persists, and additional thin fibers have been added to the alveolar region generating an increasingly complex network (Fig. 4C). These observations suggest that rather than being laid down by myofibroblasts at the onset of alveologenesis, the elastin network was present prior to alveologenesis initiates, and was remodeled into organized scaffolds for nascent septae.

Supplementary material related to this article can be found online at http://dx.doi.org/10.1016/j.ydbio.2015.11.017.

2.5. Disorganized elastin network is often, but not always associated with impaired alveologenesis

To determine if altered elastin matrix is associated with defective alveologenesis, we analyzed our mutant models and the hyperoxia model of BPD (Fig. 5). Elastin staining in *Pecam-1* mutants was similar to controls (data not shown). In contrast, *Shhcre;Etv4;5* and *Tbx4cre;Pdgfra* mutant lungs as well as hyperoxia-exposed lungs all exhibited a disorganized elastin fiber network, in interestingly distinct patterns from each other (Fig. 5A–F). In *Shhcre;Etv4;5* mutants, fibers were thin, tortuous and unraveled in all regions (Fig. 5A and B). In *Tbx4cre;Pdgfra* mutants, fibers formed a diffused mesh with minimal organization in all regions (Fig. 5C and D). Hyperoxia-exposed lungs showed patches of dense elastin mesh, with normally remodeled thick bundles in other regions (Fig. 5E and F). These data suggest that alterations in elastin fiber remodeling are often associated with impairments in alveologenesis.

2.6. Relationship between PDGFRA-GFP$^+$ fibroblasts, AEC2s, pericytes and lipids in the alveolus

In the adult lung, PDGFRA-GFP$^+$ cells, particularly those with high levels of GFP expression, reside adjacent to AEC2s, and have been suggested to serve as a stem cell niche for AEC2s (Barkauskas et al., 2013). In vitro culture experiments show that addition of epithelial cells to fetal lung mesenchyme drives up 3D septae-like structures with AEC2s in proximity to myofibroblasts (Greer et al., 2014). We sought to address whether a close relationship exists between these two cell types endogenously during development of alveoli in 3D. First, we assessed the numbers of each cell type per alveolus at P7 (Fig. 6A–C).

There were on average 7 PDGFRA-GFP+ fibroblasts (6.87 ± 2.47 cells) per alveolus. Approximately 69% of the nuclei of these cells residing near the AER, similar to previous estimation (Fig. 6A, C, Movie S5) (McGowan et al., 2008). For AEC2s, quantified by SPC staining, on average 3 cells (3.00 ± 0.94 cells) were observed in each alveolus, and there is no bias of localization near the AER (Fig. 6B and C, Movie S6). Thus, the ratio of AEC2s to PDGFRA-GFP+ fibroblasts per alveolus is approximately 1: 2.3 at P7.

Supplementary material related to this article can be found online at http://dx.doi.org/10.1016/j.ydbio.2015.11.017.

Next, we sought to determine whether a spatial relationship exists between these two cell types during development in 3D. At P0, P7 and P15, AEC2s were sometimes observed in close proximity to not only high PDGFRA-GFP$^+$ cells, but also low PDGFRAGFP cells (Fig. 6D–F, Movies S7–S9). However, AEC2s not sharing a close spatial relationship with PDGFRA-GFP$^+$ cells were also observed at all three stages (Fig. 6D–F, arrowheads, Movies S7–S9). Since PDGFRA-GFP$^+$ only labels the nuclei of these fibroblasts, we also assessed whether AEC2s are closely associated with the cytoplasmic extensions of fibroblasts. We used α-SMA to label extensions of fibroblasts, which we found is expressed by all PDGFRA-GFP$^+$ cells at P7 (Fig. 2B). AEC2s did not appear to share a pronounced spatial relationship with α-SMA$^+$ fibers at P7, although the two labels were sometimes observed near one another (Fig. 6G, Movie S10).

Supplementary material related to this article can be found online at http://dx.doi.org/10.1016/j.ydbio.2015.11.017.

We also addressed the relationship between PDGFRA-GFP$^+$ expression and PDGFRβ expression patterns in the alveoli. The latter has been implicated as a marker for pericytes. Comparison of GFP and anti-PDGFRβ antibody staining at P7 showed that there are cells with double labeling, and cells with each of the single labeling, suggesting that these two markers show overlapping but non-identical expression patterns (Fig. 6H and I).

Finally, in the adult lung, high PDGFRA-GFP fibroblasts are thought to represent a population of lipid droplet containing fibroblasts, referred to as lipofibroblasts (Barkauskas et al., 2013; Chen et al., 2012). Furthermore, lipofibroblasts have been suggested to transfer lipids to AEC2s, which can be used for surfactant production (Gewolb and Torday, 1995; Schultz et al., 2002; Torday et al., 1995). For these reasons, we next characterized the lipid contents of PDGFRA-GFP$^+$ alveolar fibroblasts using the lipid droplet dye LipidTOX (Fig. 6H and I). At P0, lipid droplet containing cells were observed in the future alveolar region (Fig. 6H, Movie S11). However, many PDGFRA-GFP+ fibroblasts were not closely associated with lipid droplets (Fig. 6H, arrowheads). By P15 the overall lipid content within the alveolar region appeared to be greatly increased (Fig. 6I, Movie S12). Surprisingly, nearly every PDGFRA-GFP$^+$ cell, not just the high GFP cells, contained LipidTOX$^+$ lipid droplets, in contrast to the finding in the adult lung (Barkauskas et al., 2013). These data raise the possibility that PDGFRA-GFP$^+$ fibroblasts undergo a developmental shift to increase lipid droplet production during alveologenesis.

Supplementary material related to this article can be found online at http://dx.doi.org/10.1016/j.ydbio.2015.11.017.

3. Discussion

Alveologenesis and the cells involved have been widely studied in 2D. However, few have studied the process in 3D over time (McGowan et al., 2008; Mund et al., 2008; Schittny et al., 2008). We reasoned that 3D reconstruction is essential for full representation of the cellular architecture, given the extensive thinning and spreading of cells after birth. In order to preserve alveolar structures, we imaged thick vibratome sections, which required minimal processing compared to other methods (paraffin sectioning, cryosectioning, plastic sectioning). Combining genetic labeling, immunofluorescent staining, confocal optical sectioning, and 3D reconstruction approaches allowed us to visualize the intricate networks of α-SMA and elastin matrices, as well as the spatial relationship between cell populations.

Our 3D images revealed that septal crests, the finger-like protrusions commonly labeled in 2D to represent newly growing septae, are often sections through existing alveolar walls (Figs. 1 and 7). These results are consistent with the findings of Mund et al., 2008 and Schittny et al., 2008, which used 3D synchrotron X-ray tomography to visualize the architecture of the luminal alveolar surface at multiple postnatal stages. Together, the data indicate that a more accurate representation of the growing septae are elongated ridges in 3D, which appear to rise up from the base of alveolar cups to subdivide the alveoli into smaller units. We have referred to these structures as septal ridges (Fig. 7). Our 3D immunostaining results indicate that during new septae formation, these ridges are underlined by α-SMA-positive myofibroblasts and associated elastin fibers.

How we define the growing septae has important implications on how we apprehend the driving force for the alveologenesis process. Based on the 2D septal crest definition, a model was put forth which postulates that myofibroblasts, after been scattered around the alveolar wall, are repelled into the lumen, pushing in the other cell types to form isolated protrusions (Burri, 1984; Lindahl et al., 1997; Prodhan and Bernard Kinane, 2002). In contrast, the 3D view of septal ridge is more compatible with a hypothesis first put forth by J.L. Emery in 1970, where he stipulated that the interlacing fibers of the elastic tissue forms a complex “fishnet” around the alveolus (Emery, 1970). Our 3D images of not just the elastin fiber, but also the myofibroblast α-SMA are consistent with the fishnet pattern. This pattern evokes a very different model of alveologenesis, where the strings of the fishnet will underlie the future alveolar ridges. Through either active constriction of the net and/or passive push by air pressure, the septal walls not lined by the fishnet will bulge out through the pores rimmed by the strings, result in relative rise of the ridges into the lumen (Fig. 7A and B). Compared to normal lung, the 3D patterns observed from some of the BPD models, for example the hyperoxia model and *Etv* mutant, indicate an increase and disorganization of α-SMA and elastin fibers. This converts the “fishnet” into a “cheese cloth”, which would be ineffective at driving the differential rise of the septal ridges from the septal walls (Fig. 7D). Thus, the 3D patterns offer testable hypotheses for the role of myofibroblasts in not just normal alveologenesis, but also in abnormal alveologenesis in BPD models.

3.1. Myofibroblasts and α-SMA fibers

In various tissues, including the lung, myofibroblasts form actin stress fibers containing α-SMA, and contract (Adler et al., 1989; Balestrini et al., 2012; Hinz, 2007; Kapanci et al., 1974; Leslie et al., 1992; Noguchi et al., 1989; Tojkander et al., 2012). In cultured lung myofibroblasts, α-SMA level is directly related to contractile force (Arora et al., 1999; Chen et al., 2012). In a pneumonectomy model of adult lung regrowth and regeneration, α-SMA induction in contractile fibroblasts is thought to drive new septae formation (Chen et al., 2012). Our results show that during alveologenesis, the timing of α-SMA induction and localization under septal ridges is consistent with a role for myofibroblast contraction in septation (Figs. 1 and 2). Furthermore, we found that at P7, all PDGFRA-GFP$^+$ cells express α-SMA. This suggests that at the height of septae formation, these cells acquire contractile property regardless of whether they belong to the PDGFRA-GFP$^+$ bright or dim populations (Fig. 2B, S2B$_i$).

Induction of α-SMA expression is often referred to as a primary step in myofibroblast differentiation. In contrast to the expectation that α-SMA stays on once activated, we found that α-SMA fiber is detected in PDGFRA-GFP+ cells during a restricted time window in development (~P2–P12). Sustained or upregulated α-SMA is associated with various impaired alveologenesis models, including both genetic and hyperoxic-exposure models (Fig. 3). Furthermore, others have shown that α-SMA expression can be reactivated during lung regrowth and regeneration (Chen et al., 2012; Perl and Gale, 2009). Together, these data suggest that rather than defining the fate of differentiated myofibroblasts, α-SMA expression may represent a contractile phenotype that the PDGFRA$^+$ cell can adopt transiently during septation, stress, or regeneration. Characterizing the mechanisms that govern α-SMA appearance and disappearance will enable future understanding of the dynamics of myofibroblast function.

In the *Pdgfa* mutant lung, PDGFRA$^+$ cells stay in clumps at the openings of saccules instead of being distributed around and getting in position for septae formation (Lindahl et al., 1997; McGowan et al., 2008; Perl and Gale, 2009). It was proposed that PDGFA signaling is primarily mediated through PDGFRA (Boström et al., 1996; Lindahl et al., 1997; McGowan et al., 2008). However, in *Tbx4cre;Pdgfra* mutants, the PDGFRA$^+$ cells are dispersed throughout the alveolar region (Fig. 3E and F, S5). This difference in phenotype is possibly due to either incomplete gene inactivation in the *Pdgfra* conditional mutants, or residual PDGFA signaling through additional receptors such as PDGFRB which shows overlapping expression with PDGFRA (Fig. 6H and I).

4. Elastin

Elastin is indispensable to lung maturation and function. Mice homozygous for the elastin null allele exhibit dilated saccules due to a defect in primary septae formation. The mutants die within a few days after birth, prior to the onset of alveologenesis (Wendel et al., 2000). Mice heterozygous for the elastin null allele show reduced lung recoil and are more susceptible to alveolar destruction from cigarette smoke in an emphysema model (Shifren et al., 2007). Furthermore, mice with mutations in various elastinogenesis pathway components display simplification of alveolar structures (reviewed in Wagenseil and Mecham (2007)).

Some models of alveologenesis have proposed that *de novo* elastin deposition at the tips of septal crests is the driving force for the formation of new septae (Boström et al., 1996; Burri, 1984; Emery, 1970; Noguchi et al., 1989). However, we observed that elastin fibers are already present at birth. A primary change in the elastin matrix between birth and the peak of alveologenesis (P7) is remodeling of these thin, widely distributed elastin fibers into thicker, more localized bundles surrounding alveolar openings. Addition of new fibers also likely occurs, and continues following the peak of alveologenesis (~P7), thereby increasing the density of the network as observed at P15 (Fig. 4C). The dynamic changes in staining pattern is consistent with previous data that in the lung, the expression of tropoelastin, the elastin monomer which is the building block of elastin fibers, decreases shortly after birth prior to the onset of alveologenesis, and increases again starting at P7, and peaks at P10–14 (Bruce and Honaker, 1998; Mariani et al., 2002). Thus, controlled deposition and remodeling of the elastin network likely work together to facilitate septae formation.

Interestingly, this remodeling of the elastic fiber network coincides with appearance of α-SMA in the alveolar region and thus presumed contractility of myofibroblasts. In other tissues, similar scenarios have been shown where myofibroblasts undergo a contractile phase and exhibit stress fiber formation during extracellular matrix and connective tissue remodeling (Hinz et al., 2012; Pellegrin and Mellor, 2007). Therefore, we hypothesize that the early elastin matrix established at birth provides a scaffold for myofibroblasts to adhere on as they drive in new septae. These contractile myofibroblasts may in turn remodel the matrix, as well as deposit new elastin fibers to rings surrounding the openings of alveoli to stabilize the nascent structures (Fig. 7E).

This crosstalk between the contractile properties of myofibroblasts and the mechanical properties of the ECM is also reflected in the finding that in several of our mutant models and our hyperoxia-exposure model of impaired alveologenesis, there is both an increases in α-SMA staining as well as disorganization of elastic fiber matrices. Currently, it is unclear whether alterations in α-SMA expression and elastic fiber organization are results of impaired lung maturation or are contributors to pathogenesis. Nevertheless, disorganization of the elastin fibers is of particular relevance to BPD as reduced lung elastance, which leads to increased effort to breathe, is a common feature of the disease.

4.1. Two waves of alveologenesis

In this study, we show that there are two phases of myofibroblast behavior in alveologenesis. In the first phase (P2–P14), myofibroblasts express α-SMA$^+$ fibers and the elastin network is remodeled (Figs. 2, 4, S1). In the second phase (P15 and later), there is no alveolar α-SMA while the elastic fiber matrix continues to increase in complexity through addition of smaller intervening fibers. The timing of this transition correlates closely with that in a two-wave model of alveologenesis (Boucherat et al., 2007; Mariani et al., 2002; Mund et al., 2008; Schittny et al., 2008). It was defined that the first wave involves rapid formation of new septal walls and the second wave involves lifting of septae off existing walls (Mund et al., 2008; Schittny et al., 2008). Our results provide clear evidence indicating that the cellular mechanisms driving the two waves of alveologenesis may be distinct.

4.2. Myofibroblasts, lipofibroblasts and AEC2s

Our observation is consistent with the notion that PDGFRA$^+$ cells show dynamic changes of characteristics in the early postnatal period. At P0, prior to the onset of alveologenesis, PDGFRA-GFP$^+$ cells in the future alveolar region lack α-SMA expression (Fig. 2A) and only a few contain lipid droplets (Fig. 6J, Movie S11). By P7, when alveolar formation is peaking, all PDGFRA-GFP$^+$ cells express α-SMA (Fig. 2B), thereby exhibiting a myofibroblast phenotype. Finally, by P15, PDGFRA-GFP$^+$ cells no longer express α-SMA (Fig. 2C) but all appear to be associated with lipid droplets (Fig. 6K, Movie S12). These results are consistent with previous findings (McGowan et al., 2008), and raise the possibility that the PDGFRA-GFP$^+$ population may differentiate into myofibroblasts with contractile-like properties during alveologenesis and then later adopt a lipofibroblast fate. However, lineage-tracing experiments need to be conducted to determine if the same cell population adopts the two different characteristics at different time points.

In adult lungs, AEC2s can be found in close proximity to PDGFRA-GFP$^+$ high-intensity, but not low-intensity fibroblasts containing lipid droplets (Barkauskas et al., 2013). Additionally, PDGFRA-GFP+ cells can promote proliferation and differentiation of AEC2s into AEC1s in alveolosphere co-cultures that mimic alveolar structures. These findings led to the proposal that PDGFRA-GFP$^+$ lipofibroblasts serve as a stem cell niche for AEC2s. Our results show that at P7, the peak of alveolar development when PDGFRA-GFP$^+$ cells are primarily myofibroblasts in character, only a subset of AEC2s are closely associated with PDGFRA-GFP$^+$ cells. The proximity of these cells increases by P15 when PDGFRA-GFP$^+$ cells are no longer SMA+, but have increased in lipid content (Fig. 6D–F). Additionally, this close apposition can be found regardless of PDGFRA-GFP$^+$ intensity level, in contrast to the selected association with high-intensity PDGFRA-GFP$^+$ cells in the adult. A further difference is that during normal development there are approximately 2.3 PDGFRA-GFP$^+$ cells for every AEC2 in each alveolus (Fig. 6C), rather than the 20:1 ratio typically used in alveolosphere co-culture experiments involving adult cells (Barkauskas et al., 2013). It awaits to be tested if PDGFRA-GFP$^+$ cells provide a trophic effect for AEC2s during alveologenesis, similar to their role in the adult lung. Furthermore, from epithelial and mesenchymal cell co-culture experiments, it was proposed that during alveologenesis, AEC2 cells may squeeze and repel myofibroblasts toward the lumen, driving out new septae (Greer et al., 2014). Our observations from the relative positioning of AEC2s and PDGFRA + myofibroblasts are in line with this proposal.

Our findings from this study re-enforce the notion that the structural and cellular composition of the alveolus is more accurately represented in 3D than in 2D. The alveologenesis process is also very dynamic, thus multiple time points need to be analyzed to fully illustrate normal or pathological conditions. Our results reveal that myofibroblasts are very sensitive to genetic and environmental perturbations, and disruption of their number and organization may in turn prevent septal formation. A comprehensive understanding of the dynamic alveologenesis process in 3D will ultimately reveal the complex causes of neonatal diseases such as BPD.

5. Experimental procedures

5.1. Animals and tissues

For wild-type studies, lungs were obtained from FVB mice between postnatal days 0 and 15. For analysis of PDGFRA-GFP, mice heterozygous for the Pdgfra-H2B-GFP allele were used (Hamilton et al., 2003; Klinghoffer et al., 2002). GFP is expressed from the endogenous *Pdgfra* locus and the expression pattern recapitulates endogenous expression of *Pdgfra* (Hamilton et al., 2003). Development of heterozygous *Pdgfra-GFP/+* mice was indistinguishable from wild-type mice. *Pdgfra* conditional knockouts were generated by breeding together *Tbx4cre* (Naiche et al., 2011), $Pdgfra^{Flox}$ (Tallquist and Soriano, 2003), and PDGFRA-GFP alleles to conditionally inactivate *Pdgfra* in the developing lung mesenchyme. For *Etv* conditional knockouts, *Shhcre* (Harfe et al., 2004), *Etv4* and *Etv5* alleles (Laing et al., 2000; Zhang et al., 2009) were used. PECAM mutants used have been described previously (DeLisser et al., 2006).

5.2. Hyperoxic-exposure

Hyperoxic-exposure was conducted as previously described (Balasubramaniam et al., 2007; Bozyk et al., 2012). Briefly, *Pdgfra-GFP* plugs were synchronized with Swiss Webster (SW) plugs. At P1, each *Pdgfra-GFP* litter was separated into 2 groups and each group was fostered by a SW mother. At P1, one group was placed into a chamber circulating with 75% oxygen through P15. The other group was maintained at normoxia (room air) conditions for the duration of the experiment. Fostering mothers were swapped between normoxia and hyperoxia litters every fourth day to maintain maternal health. Lungs from both normoxia and hyperoxia groups were harvested at P15.

5.3. Immunhistochemistry and imaging

Lungs were gravity fix-inflated with 4% paraformaldehyde, and then submerged in fix at 4 °C overnight. Whole lung lobes were embedded in 4% low-melt agarose and sections of 75 um thickness were prepared using a vibratome (Leica VT1000 S). Sections were incubated overnight at 4 °C with the following primary antibodies: rabbit anti-SPC [1:400] (Seven Hills Bioreagents), Syrian hamster anti-T1alpha (podoplanin) [1:200] (Developmental Studies Hybridoma Bank), SMA-Cy3 [1:500] (Sigma), Rb anti-elastin [1:400] (a generous gift from Robert Mecham), Rat anti-PECAM (CD31) [1:100] (BD Biosciences). Antibodies were diluted in a solution of phosphate buffered saline containing 1% Triton-X as permeabilization agent, which is also in washing solution. The following secondary antibodies were used: goat anti-rabbit Cy3, goat antirabbit FITC, goat anti-syrian hamster FITC, goat anti-syrian hamster Cy3, goat anti-rat Cy3 (Jackson Immuno Research Laboratories) [1:400]. For lipid staining, LipidTOX™ (Invitrogen) was used at 1:250. Sections were mounted in Vectashield (Vector Laboratories) beneath a coverslip raised with small pieces of clay to prevent compressing the tissues.

Immunostained tissues were observed with a confocal laser scanning microscope LSM 510 (Carl Zeiss, Germany) equipped with an argon laser (excitation 488 nm) and a DPS laser (excitation 561 nm). Serial optical sections were captured using a 40× Plan Neofluar oil objective with 1.30 numerical aperture over a total depth of 50 um with a 0.5 um z-step. The

xy plane resolution as calculated by 0.4 × wavelength/numerical aperture is 150.1 for green (488 nm) and 175 for red (570 nm). Three-dimensional reconstructions and movies were generated using IMARIS analysis software (Bitplane, Switzerland) with no averaging. Three-dimensional surface projections were rendered in IMARIS and shown for visualization of lung architecture. At minimum, flve images of different sections from lungs of four animals were compared for each stage and staining condition. For quantification of cells per alveolus, ten different lungs were used and 50 alveoli were counted at minimum. Results were reported as the mean cell number per alveolus ± standard deviation.

Supplementary Material

Refer to Web version on PubMed Central for supplementary material.

Acknowledgments

We would like to thank Dr. R. Mecham for the generous gift of the elastin antibody, the Laboratory for Optical and Computational Instrumentation (LOCI) at the University of Wisconsin-Madison for assistance with image reconstruction, and Alexander Haifan Day for cell quantification. This work was supported by American Heart Association predoctoral fellowship 14PRE20490146 and NIH predoctoral training grant T32 GM007133 (to K.B.), and by NHLBI RO1 HL113870, HL097134, March of Dimes 6-FY10-339, and Wisconsin Partnership Program grant 2897 (to X.S.).

References

Adler KB, Low RB, Leslie KO, Mitchell J, Evans JN. Contractile cells in normal and fibrotic lung. Lab. Invest. 1989; 60:473–485. [PubMed: 2651799]

Amy RW, Bowes D, Burri PH, Haines J, Thurlbeck WM. Postnatal growth of the mouse lung. J. Anat. 1977; 124:131–151. [PubMed: 914698]

Arora PD, Narani N, McCulloch CA. The compliance of collagen gels regulates transforming growth factor-beta induction of alpha-smooth muscle actin in fibroblasts. Am. J. Pathol. 1999; 154:871–882. [PubMed: 10079265]

Askie LM, Henderson-Smart DJ, Irwig L, Simpson JM. Oxygen-saturation targets and outcomes in extremely preterm infants. N. Engl. J. Med. 2003; 349:959–967. [PubMed: 12954744]

Aslam M, Baveja R, Liang OD, Fernandez-Gonzalez A, Lee C, Mitsialis SA, Kourembanas S. Bone marrow stromal cells attenuate lung injury in a murine model of neonatal chronic lung disease. Am. J. Respir. Crit. Care Med. 2009; 180:1122–1130. [PubMed: 19713447]

Balasubramaniam V, Mervis CF, Maxey AM, Markham NE, Abman SH. Hyperoxia reduces bone marrow, circulating, and lung endothelial progenitor cells in the developing lung: implications for the pathogenesis of broncho-pulmonary dysplasia. Am. J. Physiol. Lung Cell. Mol. Physiol. 2007; 292:L1073–L1084. [PubMed: 17209139]

Balestrini JL, Chaudhry S, Sarrazy V, Koehler A, Hinz B. The mechanical memory of lung myofibroblasts. Integr. Biol. 2012; 4:410.

Barkauskas CE, Cronce MJ, Rackley CR, Bowie EJ, Keene DR, Stripp BR, Randell SH, Noble PW, Hogan BLM. Type 2 alveolar cells are stem cells in adult lung. J. Clin. Invest. 2013; 123:3025–3036. [PubMed: 23921127]

Boström H, Gritli-Linde A, Betsholtz C. PDGF-A/PDGF alpha-receptor signaling is required for lung growth and the formation of alveoli but not for early lung branching morphogenesis. Dev. Dyn. 2002; 223:155–162. [PubMed: 11803579]

Boström H, Willetts K, Pekny M, Levéen P, Lindahl P, Hedstrand H, Pekna M, Hellström M, Gebre-Medhin S, Schalling M, Nilsson M, Kurland S, Törnell J, Heath JK, Betsholtz C. PDGF-A signaling is a critical event in lung alveolar myofibroblast development and alveogenesis. Cell. 1996; 85:863–873. [PubMed: 8681381]

Boucherat O, Franco-Montoya M-L, Thibault C, Incitti R, Chailley-Heu B, Delacourt C, Bourbon JR. Gene expression profiling in lung fibroblasts reveals new players in alveolarization. Physiol. Genom. 2007; 32:128–141.

Bozyk PD, Bentley JK, Popova AP, Anyanwu AC, Linn MD, Goldsmith AM, Pryhuber GS, Moore BB, Hershenson MB. Neonatal periostin knockout mice are protected from hyperoxia-induced alveolar simplication. PLoS One. 2012; 7:1–10.

Brody JS, Kaplan NB. Proliferation of alveolar interstitial cells during postnatal lung growth. Evidence for two distinct populations of pulmonary fibroblasts. Am. Rev. Respir. Dis. 1983; 127:763–770. [PubMed: 6859658]

Bruce MC, Honaker CE. Transcriptional regulation of tropoelastin expression in rat lung fibroblasts: changes with age and hyperoxia. Am. J. Physiol. 1998; 274:L940–L950. [PubMed: 9609733]

Burri P, Weibel E. Ultrastructure and morphometry of the developing lung. Development of the Lung. 1977

Burri PH. Fetal and postnatal development of the lung. Annu. Rev. Physiol. 1984; 46:617–628. [PubMed: 6370120]

Chen L, Acciani T, Le Cras T, Lutzko C, Perl A-KT. Dynamic regulation of platelet-derived growth factor receptor α expression in alveolar fibroblasts during realveolarization. Am. J. Respir. Cell. Mol. Biol. 2012; 47:517–527. [PubMed: 22652199]

Churg AM, Tazelaar HD, Myers JL, Wright JL. Thurlbeck's Pathology of the Lung. 2005

DeLisser HM, Helmke BP, Cao G, Egan PM, Taichman D, Fehrenbach M, Zaman A, Cui Z, Mohan GS, Baldwin HS, Davies PF, Savani RC. Loss of PECAM-1 function impairs alveolarization. J. Biol. Chem. 2006; 281:8724–8731. [PubMed: 16377626]

Dunnill MS. Postnatal growth of the lung. Thorax. 1962; 17:329–333.

Emery JL. The post natal development of the human lung and its implications for lung pathology. Respiration. 1970; 27:41–50. [PubMed: 5511279]

Gewolb IH, Torday JS. High glucose inhibits maturation of the fetal lung in vitro. Morphometric analysis of lamellar bodies and fibroblast lipid inclusions. Lab. Invest. 1995; 73:59–63. [PubMed: 7603041]

Greer RM, Miller JD, Okoh VO, Halloran BA, Prince LS. Epithelial-mesenchymal co-culture model for studying alveolar morphogenesis. Organogenesis. 2014; 10:340–349. [PubMed: 25482312]

Hamilton TG, Klinghoffer RA, Corrin PD, Soriano P. Evolutionary divergence of platelet-derived growth factor alpha receptor signaling mechanisms. Mol. Cell. Biol. 2003; 23:4013–4025. [PubMed: 12748302]

Harfe BD, Scherz PJ, Nissim S, Tian H, McMahon AP, Tabin CJ. Evidence for an expansion-based temporal Shh gradient in specifying vertebrate digit identities. Cell. 2004; 118:517–528. [PubMed: 15315763]

Herriges JC, Verheyden JM, Zhang Z, Sui P, Zhang Y, Anderson MJ, Swing DA, Zhang Y, Lewandoski M, Sun X. FGF-regulated ETV transcription factors control FGF-SHH feedback loop in lung branching. Dev. Cell. 2015; 35:322–332. [PubMed: 26555052]

Hinz B. Formation and function of the myofibroblast during tissue repair. J. Invest. Dermatol. 2007; 127:526–537. [PubMed: 17299435]

Hinz B, Phan SH, Thannickal VJ, Prunotto M, Desmoulière A, Varga J, De Wever O, Mareel M, Gabbiani G. Recent developments in myofibroblast biology: paradigms for connective tissue remodeling. Am. J. Pathol. 2012; 180:1340–1355. [PubMed: 22387320]

Husain AN, Siddiqui NH, Stocker JT. Pathology of arrested acinar development in postsurfactant bronchopulmonary dysplasia. Hum. Pathol. 1998; 29:710–717. [PubMed: 9670828]

Jobe AH, Bancalari E. Bronchopulmonary Dysplasia. Am. J. Respir. Crit. Care Med. 2001; 163:1723–1729. [PubMed: 11401896]

Jobe AJ. The new BPD: an arrest of lung development. Pediatr. Res. 1999; 46:641–643. [PubMed: 10590017]

Kapanci Y, Assimacopoulos A, Irle C, Zwahlen A, Gabbiani G. "Contractile interstitial cells" in pulmonary alveolar septa: a possible regulator of ventilation/perfusion ratio. J. Cell. Biol. 1974; 60:375–392. [PubMed: 4204972]

Kimani PW, Holmes AJ, Grossmann RE, McGowan SE. PDGF-Ralpha gene expression predicts proliferation, but PDGF-A suppresses transdifferentiation of neonatal mouse lung myofibroblasts. Respir. Res. 2009; 10:119. [PubMed: 19939260]

Klinghoffer RA, Hamilton TG, Hoch R, Soriano P. An allelic series at the PDGFαR locus indicates unequal contributions of distinct signaling pathways during development. Dev. Cell. 2002; 2:103–113. [PubMed: 11782318]

Laing MA, Coonrod S, Hinton BT, Downie JW, Tozer R, Rudnicki MA, Hassell JA. Male sexual dysfunction in mice bearing targeted mutant alleles of the PEA3 ets gene. Mol. Cell. Biol. 2000; 20:9337–9345. [PubMed: 11094084]

Langston C, Kida K, Reed M, Thurlbeck WM. Human lung growth in late gestation and in the neonate. Am. Rev. Respir. Dis. 1984; 129:607–613. [PubMed: 6538770]

Leslie K, Mitchell J, Low R. Views and reviews lung myofibroblasts. Cell Motil. Cytoskelet. 1992; 98:92–98.

Leslie KO, Mitchell JJ, Woodcock-Mitchell JL, Low RB. Alpha smooth muscle actin expression in developing and adult human lung. Differentiation. 1990; 44:143–149. [PubMed: 2283003]

Lindahl P, Karlsson L, Hellström M, Gebre-Medhin S, Willetts K, Heath JK, Betsholtz C. Alveogenesis failure in PDGF-A-deficient mice is coupled to lack of distal spreading of alveolar smooth muscle cell progenitors during lung development. Development. 1997; 124:3943–3953. [PubMed: 9374392]

Mariani TJ, Reed JJ, Shapiro SD. Expression profiling of the developing mouse lung. Am. J. Respir. Cell. Mol. Biol. 2002; 26:541–548. [PubMed: 11970905]

McGowan SE, Grossmann RE, Kimani PW, Holmes AJ. Platelet-Derived Growth Factor Receptor-Alpha-Expressing cells localize to the alveolar entry ring and have characteristics of myofibroblasts during pulmonary Alveolar Septal Formation. Anat. Rec. 2008; 291:1649–1661.

McGowan SE, McCoy DM. Regulation of fibroblast lipid storage and myofibroblast phenotypes during alveolar septation in mice. Am. J. Physiol. Lung Cell. Mol. Physiol. 2014; 307:L618–L631. [PubMed: 25150063]

McGowan SE, McCoy DM. Platelet-derived growth factor-A regulates lung fibroblast S-phase entry through p27(kip1) and FoxO3a. Respir. Res. 2013; 14:68. [PubMed: 23819440]

McGowan SE, Torday JS. The pulmonary lipofibroblast (lipid interstitial cell) and its contributions to alveolar development. Annu. Rev. Physiol. 1997; 59:43–62. [PubMed: 9074756]

Mitchell JJ, Reynolds SE, Leslie KO, Low RB, Woodcock-Mitchell J. Smooth muscle cell markers in developing rat lung. Am. J. Respir. Cell. Mol. Biol. 1990; 3:515–523. [PubMed: 2252578]

Mund SI, Stampanoni M, Schittny JC. Developmental alveolarization of the mouse lung. Dev. Dyn. 2008; 237:2108–2116. [PubMed: 18651668]

Naiche, La; Arora, R.; Kania, A.; Lewandoski, M.; Papaioannou, VE. Identity and fate of Tbx4-expressing cells reveal developmental cell fate decisions in the allantois, limb, and external genitalia. Dev. Dyn. 2011; 240:2290–2300. [PubMed: 21932311]

Noguchi A, Reddy R, Kursar JD, Parks WC, Mecham RP. Smooth muscle isoactin and elastin in fetal bovine lung. Exp. Lung Res. 1989; 15:537–552. [PubMed: 2767003]

Ochs M, Nyengaard JR, Jung A, Knudsen L, Voigt M, Wahlers T, Richter J, Gundersen HJG. The number of alveoli in the human lung. Am. J. Respir. Crit. Care Med. 2004; 169:120–124. [PubMed: 14512270]

Pellegrin S, Mellor H. Actin stress fibres. J. Cell. Sci. 2007; 120:3491–3499. [PubMed: 17928305]

Perl A-KT, Gale E. FGF signaling is required for myofibroblast differentiation during alveolar regeneration. Am. J. Physiol. Lung Cell. Mol. Physiol. 2009; 297:L299–L308. [PubMed: 19502291]

Prodhan P, Bernard Kinane T. Developmental paradigms in terminal lung development. BioEssays. 2002; 24:1052–1059. [PubMed: 12386936]

Ratner V, Starkov A, Matsiukevich D, Polin RA, Ten VS. Mitochondrial dysfunction contributes to alveolar developmental arrest in hyperoxia-exposed mice. Am. J. Respir. Cell. Mol. Biol. 2009; 40:511–518. [PubMed: 19168698]

Rehan VK, Sugano S, Wang Y, Santos J, Romero S, Dasgupta C, Keane MP, Stahlman MT, Torday JS. Evidence for the presence of lipofibroblasts in human lung. Exp. Lung Res. 2006; 32:379–393. [PubMed: 17090478]

Rhoades, RA.; Bell, DR. Medical Phisiology: Principles for Clinical Medicine. United States: Lippincott Williams & Wilkins; 2012.

Sanders YY, Kumbla P, Hagood JS. Enhanced myofibroblastic differentiation and survival in thy-1(−) lung fibroblasts. Am. J. Respir. Cell. Mol. Biol. 2007; 36:226–235. [PubMed: 16960126]

Saugstad OD. Bronchopulmonary dysplasia-oxidative stress and anti-oxidants. Semin. Neonatol. 2003; 8:39–49. [PubMed: 12667829]

Schittny JC, Mund SI, Stampanoni M. Evidence and structural mechanism for late lung alveolarization. Am. J. Physiol. Lung Cell. Mol. Physiol. 2008; 294:L246–L254. [PubMed: 18032698]

Schultz CJ, Torres E, Londos C, Torday JS. Role of adipocyte differentiation-related protein in surfactant phospholipid synthesis by type II cells. Am. J. Physiol. Lung Cell. Mol. Physiol. 2002; 283:L288–L296. [PubMed: 12114189]

Shifren A, Durmowicz AG, Knutsen RH, Hirano E, Mecham RP. Elastin protein levels are a vital modifier affecting normal lung development and susceptibility to emphysema. Am. J. Physiol. Lung Cell. Mol. Physiol. 2007; 292:L778–L787. [PubMed: 17142349]

Tallquist MD, Soriano P. Cell autonomous requirement for PDGFRalpha in populations of cranial and cardiac neural crest cells. Development. 2003; 130:507–518. [PubMed: 12490557]

Thurlbeck WM. Postnatal human lung growth. Thorax. 1982; 37:564–571. [PubMed: 7179184]

Tojkander S, Gateva G, Lappalainen P. Actin stress fibers-assembly, dynamics and biological roles. J. Cell. Sci. 2012; 125:1855–1864. [PubMed: 22544950]

Torday J, Hua J, Slavin R. Metabolism and fate of neutral lipids of fetal lung fibroblast origin. Biochim. Biophys. Acta. 1995; 1254:198–206. [PubMed: 7827125]

Vento M, Moro M, Escrig R, Arruza L, Villar G, Izquierdo I, Roberts LJ, Arduini A, Escobar JJ, Sastre J, Asensi MA. Preterm resuscitation with low oxygen causes less oxidative stress, inflammation, and chronic lung disease. Pediatrics. 2009; 124:e439–e449. [PubMed: 19661049]

Wagenseil JE, Mecham RP. New insights into elastic fiber assembly. Birth Defects Res. Part C-Embryo Today Rev. 2007; 81:229–240.

Wendel DP, Taylor DG, Albertine KH, Keating MT, Li DY. Impaired distal airway development in mice lacking elastin. Am. J. Respir. Cell. Mol. Biol. 2000; 23:320–326. [PubMed: 10970822]

Zeltner TB, Burri PH. The postnatal development and growth of the human lung II. Morphol. Respir. Physiol. 1987; 67:269–282.

Zhang Z, Verheyden JM, Hassell JA, Sun X. FGF-regulated Etv genes are essential for repressing Shh expression in mouse limb buds. Dev. Cell. 2009; 16:607–613. [PubMed: 19386269]

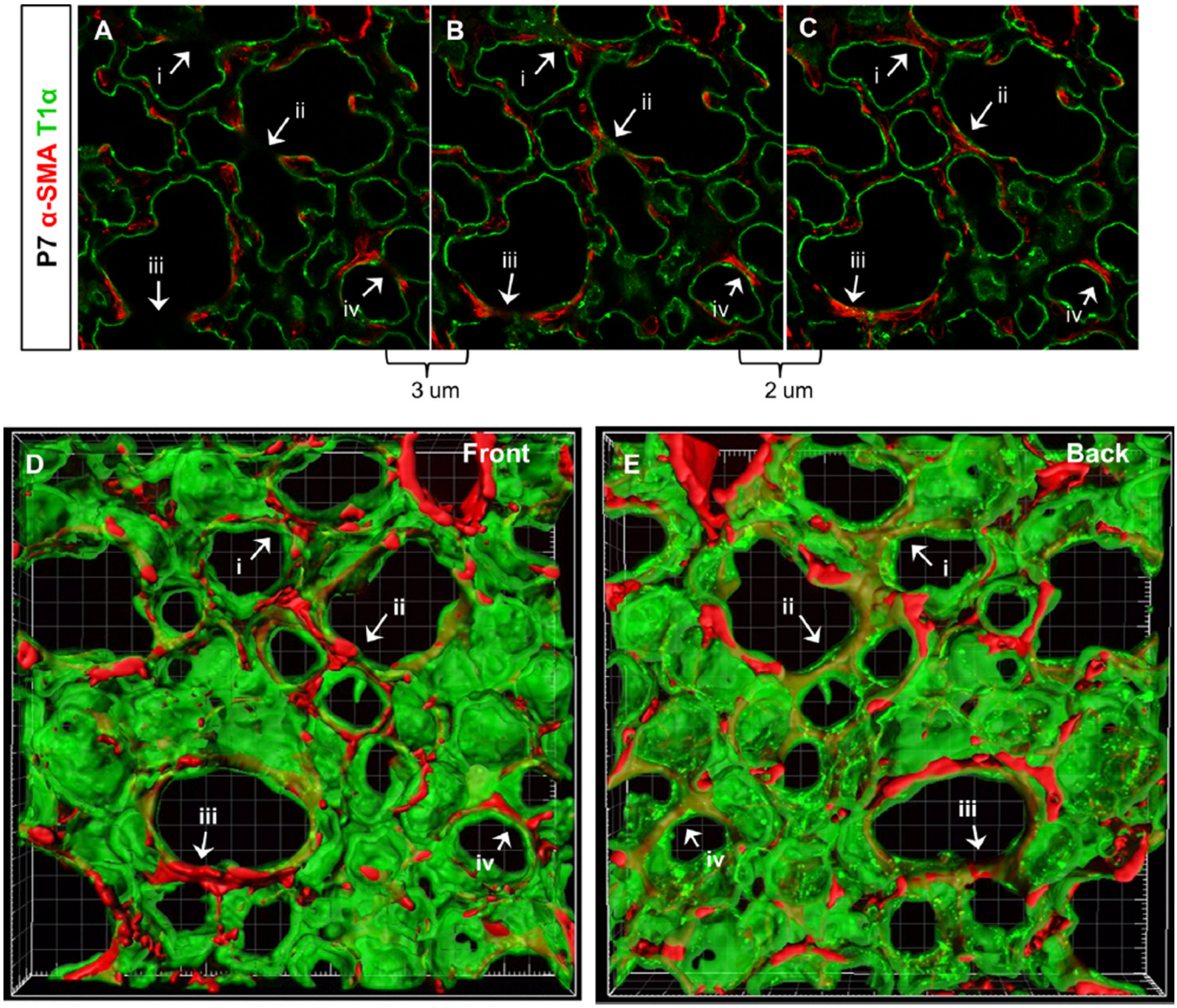

Fig. 1.

Septal crests represent sections through existing alveolar walls. (A–C) 2D images of individual optical sections of 75 μm lung slice with α-SMA and T1α staining. Optical section in (A) is 3 um above section in (B) and image (B) is 2 um above optical section in (C). Arrows (i–iv) indicate septal crests that converge into closed alveolar walls in another section plane. (D–E) Front and back views of 3D surface rendering of 50 um image stack which includes optical sections shown in (A–C) [see also Movie S1]. Arrows (i–iv) indicate alveolar walls in 3D that correspond to the 2D septal crests indicated in (A–C). (A–E) 40× magnification. All images in following figures are 3D renderings unless otherwise specified.

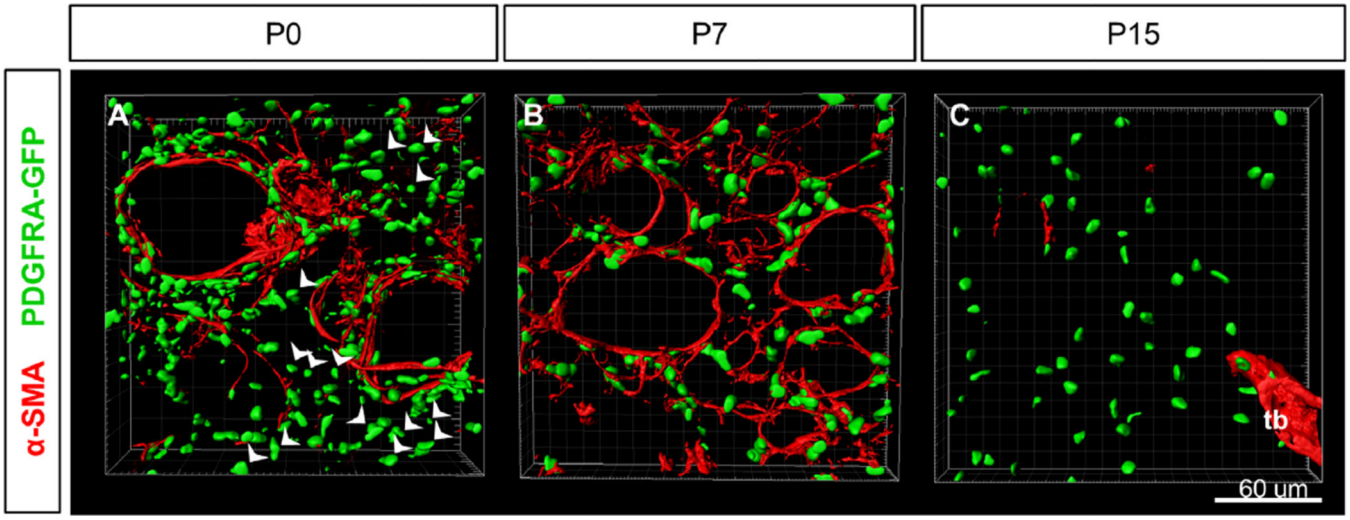

Fig. 2.

α-SMA is expressed in a restricted time window in alveoli. (A–C) Surface rendering of PDGFRA-GFP expression and α-SMA staining in alveolar region at stages P0, P7 and P15. (A) α-SMA fibers surround saccules openings and arterioles at P0. Arrowheads indicate PDGFRA-GFP^{+} cells not surrounding saccules which do not express α-SMA at P0. (B) All PDGFRA-GFP^{+} myofibroblasts are associated with α-SMA fibers surrounding alveoli at P7. (C) PDGFRA-GFP^{+} cells in the alveolar region do not express α-SMA at P15. α-SMA is expression is still found surrounding terminal bronchioles (tb). (A–C) 40× magnification.

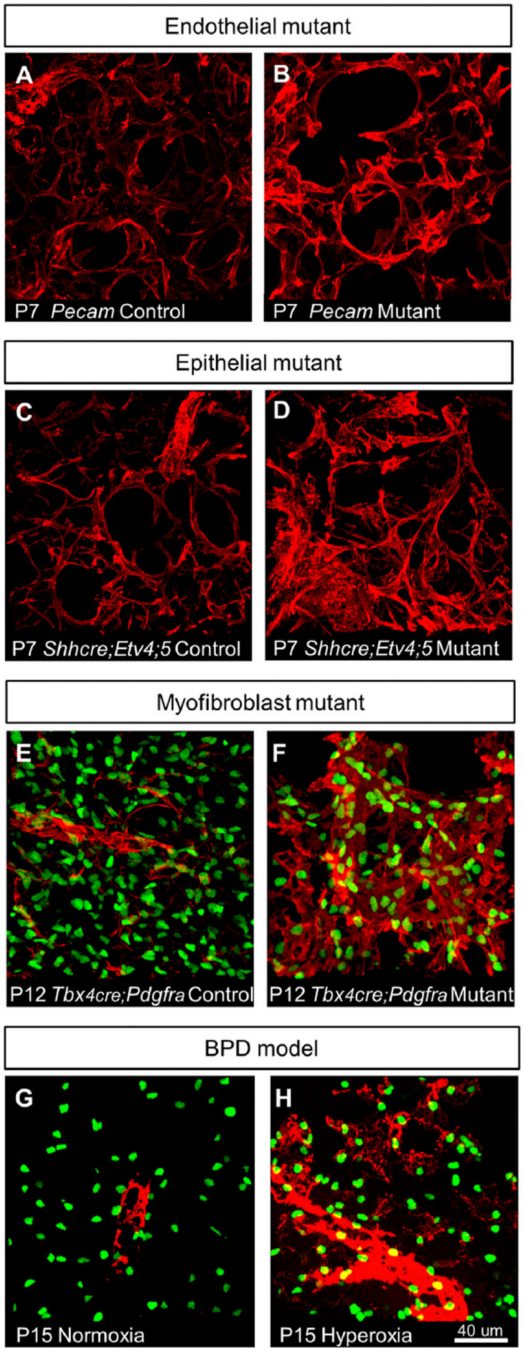

Fig. 3.

Mouse models of disrupted alveolar formation exhibit altered α-SMA expression. (A–H) α-SMA staining (red) in alveolar region. (E–H) PDGFRA-GFP labels expressing nuclei. (A–B) *Pecam-1* mutants, which exhibit impaired alveologenesis due to endothelial defects, shows increased α-SMA expression around alveoli at P7. (C–D) *Shhcre;Etv4;5* mutants, which exhibit impaired alveologenesis due to epithelial defects, shows increased α-SMA expression and disorganized fibers around alveoli at P7. (E–F) *Tbx4cre;Pdgfra* mutants, which exhibit impaired alveologenesis due to myofibroblast defects, shows increased α-

SMA expression in an expanded domain at P12. (G–H) Hyperoxia-exposed mice, which mimic alveolar defects observed in human BPD, exhibit α-SMA expression in alveolar region at P15 when normoxia-exposed alveoli no longer express α-SMA.

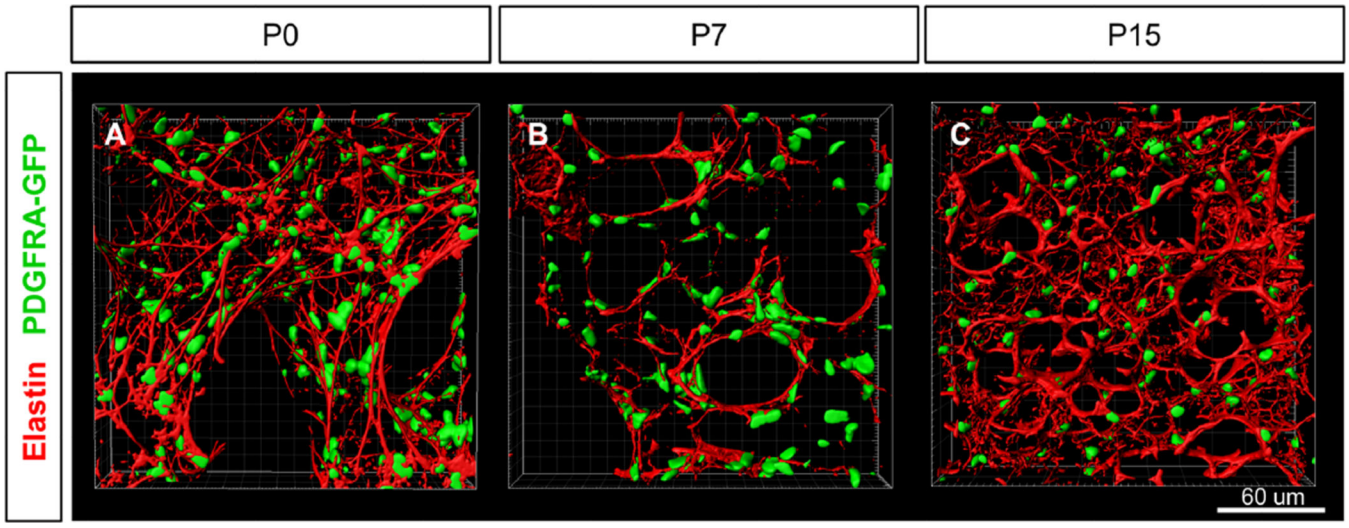

Fig. 4.

Elastin fiber matrix is present at birth and undergoes remodeling during alveologenesis. (A–C) Surface rendering of PDGFRA-GFP expression and elastin staining in alveolar region at stages P0, P7 and P15. (A) Complex elastin fiber matrix is established by P0. All PDGFRA-GFP^{+} cells appear to be associated with elastin fibers. (B) By P7, elastin matrix has been remodeled to form tight bundles and are preferentially associated with the PDGFRA-GFP cells surrounding the AER. (C) By P15, the elastin fiber matrix is more complex with additional small fibers. (A–C) 40× magnification.

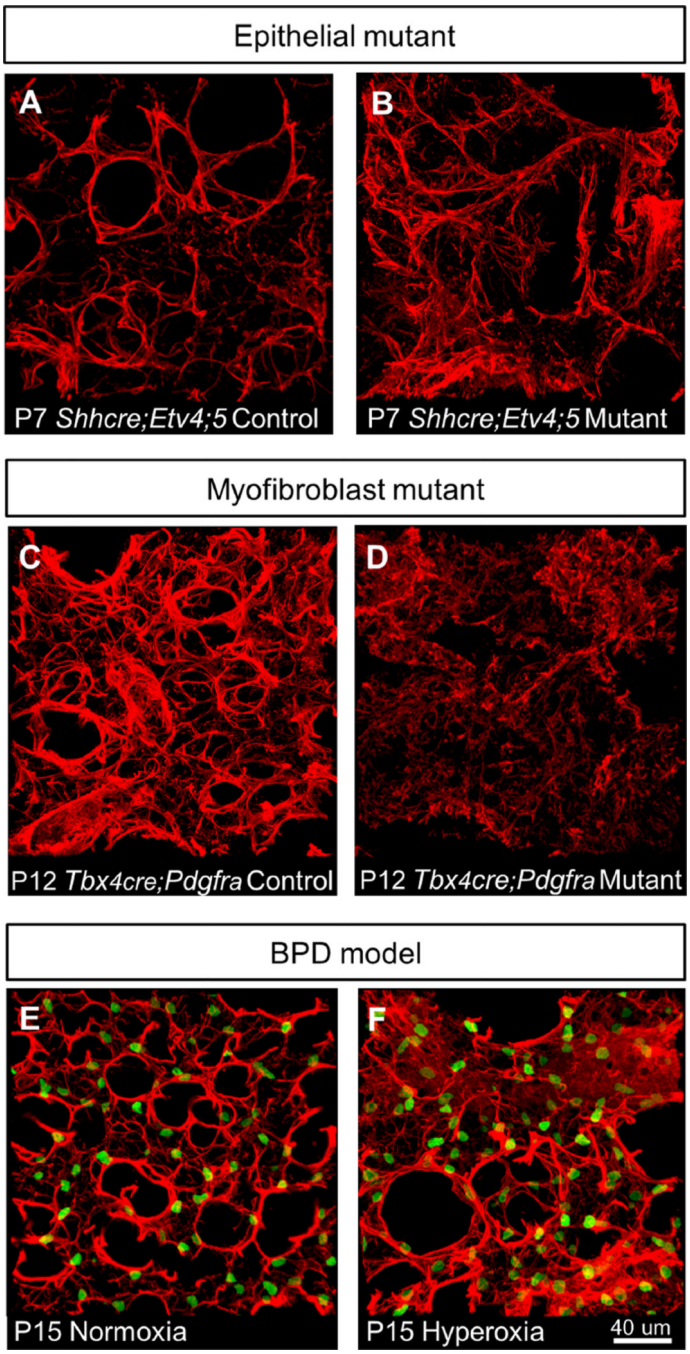

Fig. 5.

Mouse models of impaired alveologenesis exhibit disorganized elastin matrices. (A–F) Elastin staining (red) in alveolar region. (E–F) PDGFRA-GFP labels the nuclei of expressing cells. (A–B) *Tbx4cre;Pdgfra* mutants show mesh of elastin fibers lacking thick bundles at P12. (C–D) *Shhcre;Etv4;5* mutants show disorganized thin tortuous elastin fibers at P7. (E–F) Hyperoxia-exposed lungs show patches of dense elastin mesh (see top region and bottom right region of image), while other alveolar regions exhibit apparently normal elastin bundles at P15.

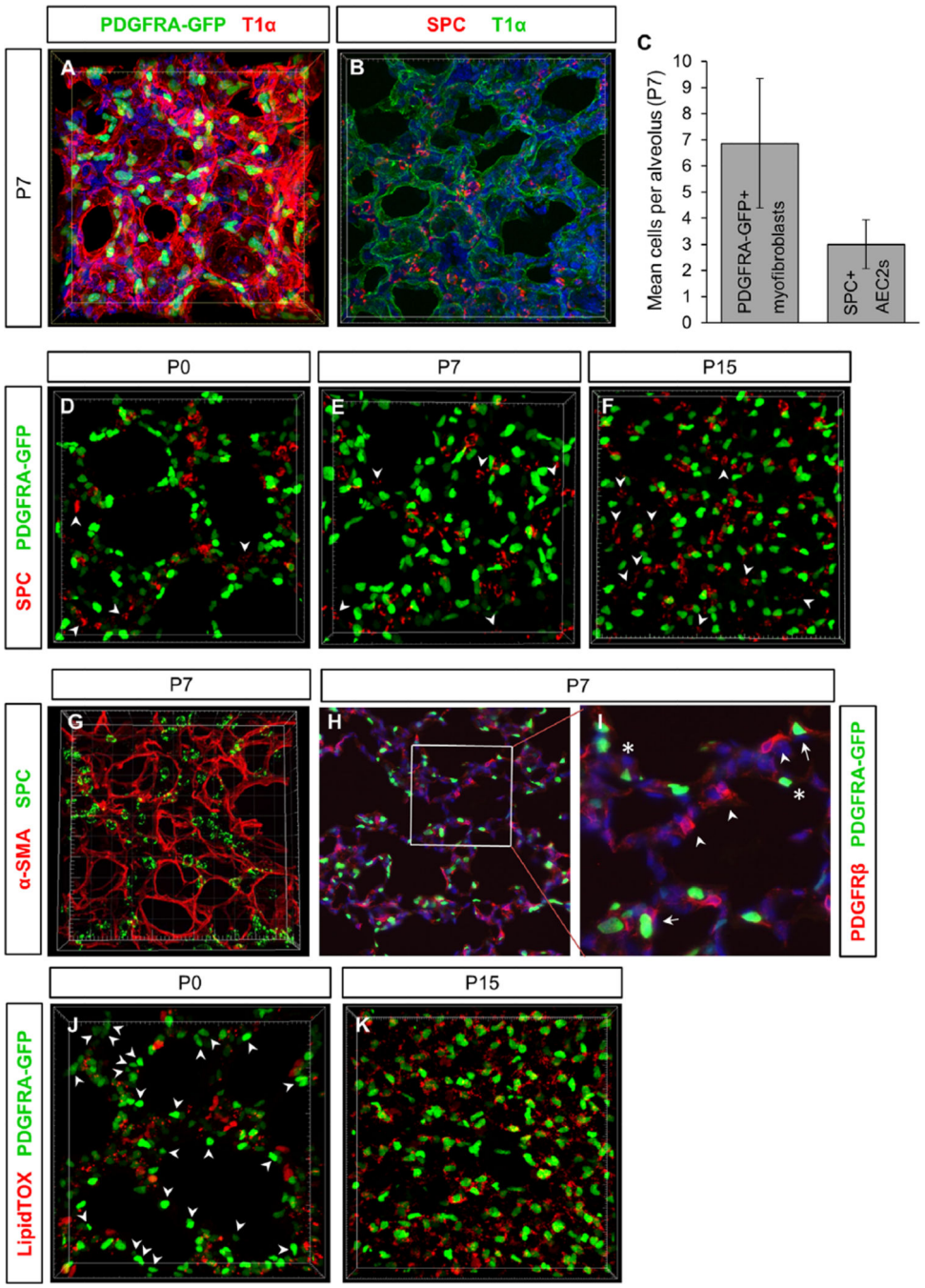

Fig. 6.

Myofibroblast relationship to AEC2s and lipid droplets. (A) PDGFRA-GFP$^+$ myofibroblasts at P7 in alveoli, outlined by T1α staining of AEC1s [see also Movie S5]. (B) AEC2s at P7 in T1α outlined alveoli [see also Movie S6]. (C) Quantification of mean myofibroblasts/alveolus and AEC2s/alveolus at P7. PDGFRA-GFP$^+$ myofibroblasts per alveolus: 6.87 cells ± 2.47. SPC$^+$ AEC2s per alveolus: 3.00 cells ± 0.94. n = 10 lungs each, minimum of 50 alveoli quantified. (D–F) PDGFRA-GFP expression and SPC staining in alveolar region at stages P0, P7 and P15 [see also Movies S7–S9]. Arrowheads indicate AEC2s that are not in

direct apposition to PDGFRA-GFP+ cell. (G) SPC and α-SMA staining at P7 [see also Movie S10]. (H,I) PDGFRA-GFP expression and anti-PDGFRβ staining in alveolar region at P7. Boxed area in H is magnified in I. Arrows indicate PDGFRA-GFP and PDGFRβ double positive cells, arrowheads indicate PDGFRβ single positive cells, asterisks indicate PDGFRA-GFP single positive cells. (J,K) PDGFRA-GFP expression and LipidTOX staining of lipid droplets at P0 and P15 [see also Movie S11 and S12]. A subset of PDGFRA-GFP^{+} cells are associated with lipid droplets at P0 (J), while all PDGFRA-GFP^{+} cells appear closely associated with lipid droplets by P15 (K). Arrowheads in (J) indicate PDGFRA-GFP^{+} cells that are not closely associated with lipid droplets.

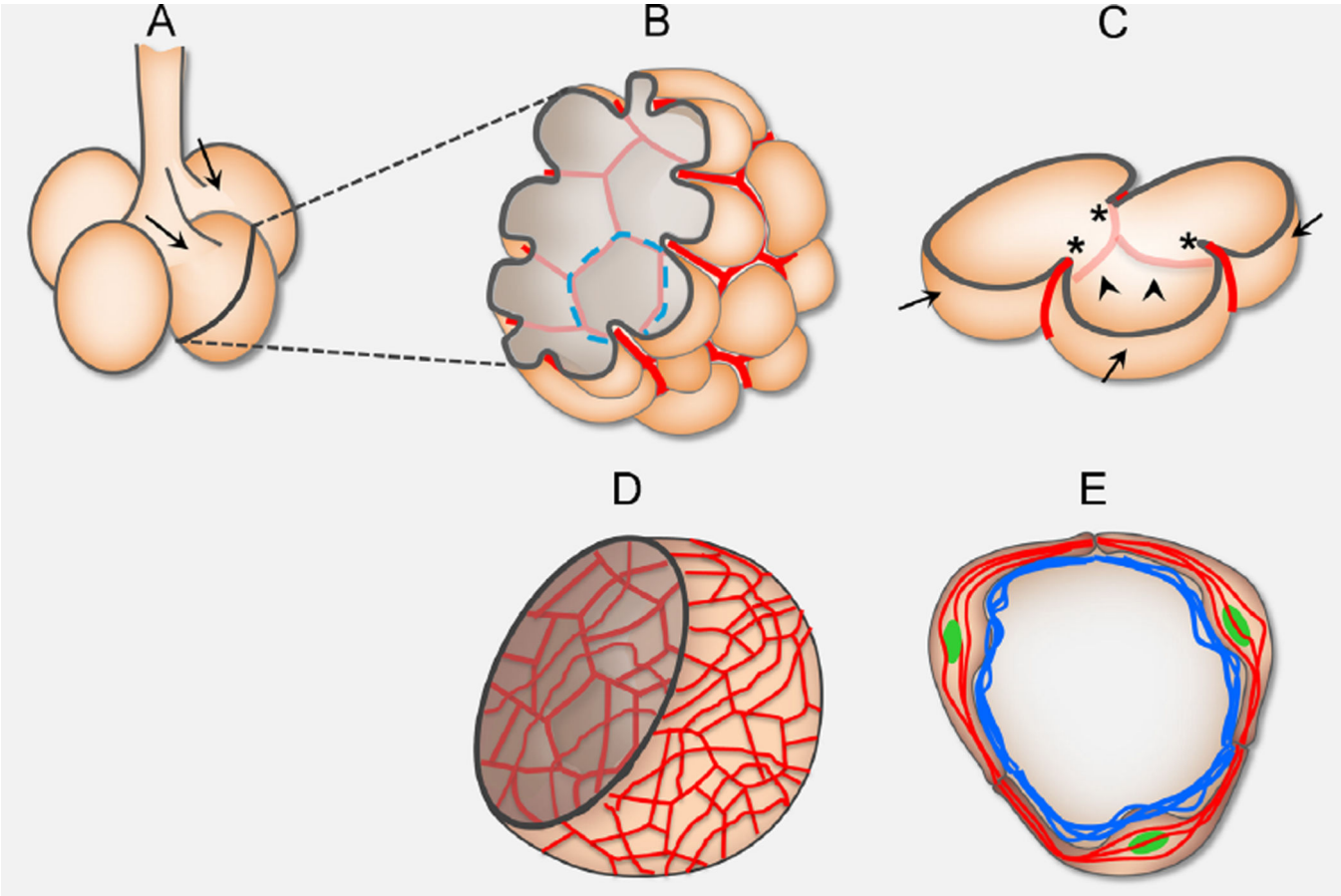

Fig. 7.

A schematic of alveologenesis. (A) At birth, prior to alveolar formation, the distal-most lung structures are saccules (shown as circular buds) which form off of terminal bronchioles. Arrows indicate saccule openings. (B) During the peak phase of alveologenesis (P4–P12), α-SMA (in red) and closely associated elastin matrices (not shown) is expressed in an organized network, mimicking a “fishnet” pattern in the alveolar region. Peach-colored hemisphere represents epithelial lining of a saccule. Dotted blue circle outlines an alveolar entrance ring (AER) that is underlined by α-SMA. (C) A slice containing several alveoli. Septal ridges (arrowheads) are lined by α-SMA fibers (in red) and closely associated elastin fibers (not shown). Top dark line outline a possible cut 2D view with septal crests (asterisks) that are a result of a section through fully grown septal walls (arrows). (D) Increase and disorganization in α-SMA (red) and elastin matrices (not shown) transforms “fishnet” into “cheese cloth” and would prevent relative rise of ridges into the lumen, thereby impair alveoli formation. (E) At the height of septae formation (P4–12), PDGFRA-GFP^{+} (green) myofibroblasts form a ring at the AER, where they express α-SMA fibers (red) and deposit elastin fibers (blue). These cells may contract as they drive in new septae, meanwhile remodeling the matrix to stabilize newly formed structures.